Applied Acoustics 73 (2012) 56–60

Contents lists available at ScienceDirect

Applied Acoustics

journal homepage: www.elsevier.com/locate/apacoust

Controlling sound absorption by an upstream resistive layer

F. Chevillotte

MATELYS, 1 rue Baumer, F69120 Vaulx-en-Velin, France

ARTICLE INFO

Article history:
Received 25 January 2011
Received in revised form 6 July 2011
Accepted 7 July 2011
Available online 11 August 2011

Keywords:
Porous media
Resistive layer
Perforated plate
Screen
Sound absorption
Multilayer
Textile
Recycled material
Microstructure

ABSTRACT

Resistive screens, or perforated plates, are widely used upstream of porous materials. They can be used either for protection or decoration, or for acoustic properties enhancement. This study points out the role that a resistive layer can have upstream on a porous material. Based on numerical simulations, this work gives the guidelines for rational use of high resistive layers in order to maximize the normal sound absorption of porous multilayers. Two major results emerge: (i) the upstream resistive layer can control the sound absorption of the porous multilayer, while nullifying the acoustic properties of downstream layer and (ii) this upstream layer may be detrimental to sound absorption of porous multilayer. Experimental validation on a porous multilayer, controlled by a woven textile, supports these findings. The sound absorption of material with poor sound absorption performance can be enhanced with a conveniently designed resistive layer.

1. Introduction

Porous materials, used as sound absorbers, are often assembled with a resistive layer. This layer can be used in order to increase acoustic properties but it is generally used for protection or decoration. Rock and glass wools, known as good sound absorbers, are often mounted with a perforated plate. This plate keeps a rigid wall while protecting the wool. Textiles (woven or non-woven) are increasingly used upstream of acoustical porous materials.

Is it possible to control the sound absorption of a porous media by adding an upstream resistive layer?

This question is addressed in this paper by focusing on a porous multilayer made of an upstream resistive layer and a downstream porous material (Fig. 1). This porous multilayer is excited by long-wavelength acoustic plane waves on normal incidence. In this work, the resistive layer is considered motionless.

After briefly describing the modeling of such resistive layers in Section 2, a simple formula, used as a guideline for design, is in Section 3. An experimental validation is finally achieved in Section 4.

2. Modeling of perforated plate

Several models have been developed for modeling perforated plates combined with air gaps or porous media [1–6]. These models aim at calculating acoustic impedance of a perforated plate backed or not by a cavity, which is filled or not with a porous media. Models have been specially formulated for unbonded and bonded facings set on porous layers [6]. A periodic hole arrangement is typically considered and the models are based on a single hole. This implies that no coupling between holes is considered and this is thus valid for low open area ratio (<10%). Circular holes are usually considered. The thin thickness of the plates and the simple hole shape allow to neglect thermal effects of acoustic energy dissipation. The main acoustic energy dissipation is due to visco-inertial effects. The plate motion can also play a role but is not taken into account in this study.

These models include a length correction due to the flow distortion around the aperture (Fig. 2). This correction is also called added length or added mass effect. One difference between the models is the way that this correction term is considered. Allard and Ingard use a modal approach in an elementary hole to calculate it [1,2,5].

Recently, Atalla and Sgard introduce a simple and general model for modeling perforated plates using a rigid frame porous model [7]. One can thus use the Johnson–Champoux–Allard (JCA) equivalent fluid model [8,9] for modeling such a perforated plate. Note that elastic parameters can be taken into account using transfer matrix method [10].

Considering a perforated plate with a thickness L, a perforation diameter D_{perf} and a fraction of open area ϕ, the viscous and thermal characteristic lengths Λ and Λ', and the resistivity σ can easily be expressed as:

E-mail address: fabien.chevillotte@matelys.com

0003-682X/$ - see front matter © 2011 Elsevier Ltd. All rights reserved.
doi:10.1016/j.apacoust.2011.07.005

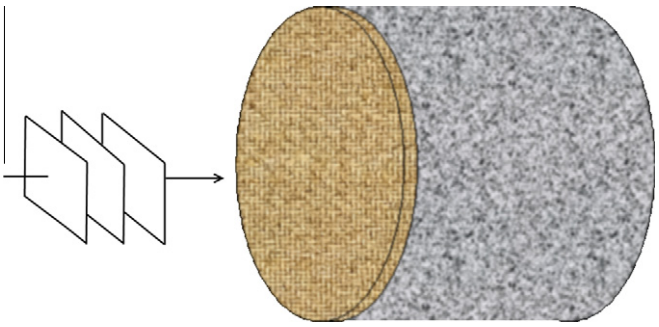

Fig. 1. Example of multilayer made up of a downstream porous media (or air cavity) and a resistive layer (screen or perforated plate).

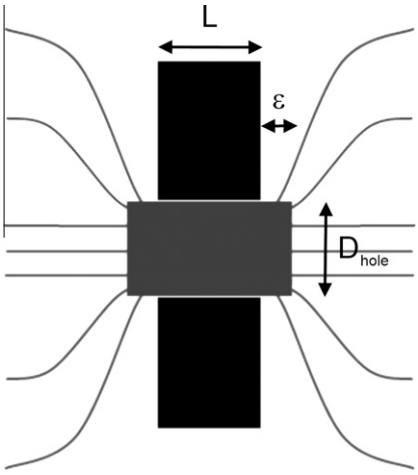

Fig. 2. Scheme of an aperture with distorted flow.

$$\Lambda = \Lambda' = \frac{D_{\text{perf}}}{2}, \tag{1}$$

and

$$\sigma = \frac{32\eta}{\phi D_{\text{perf}}^2}, \tag{2}$$

where η is the air viscosity.

The method proposed by Atalla and Sgard is taking into account the added length due to the flow distortion by modifying the tortuosity α_∞, depending on the upstream and downstream surrounding media [7]. They show that a dynamic correction of the high frequency limit of the tortuosity has to be taken into account when considering a high resistive media combined with perforated plate. This correction for a perforated plate combined with an air gap is given by:

$$\alpha_\infty(\omega) = 1 + \frac{2\varepsilon}{L}, \tag{3}$$

and

$$\alpha_\infty(\omega) = 1 + (1 + \Re(\tilde{\alpha}))\frac{\varepsilon}{L}, \tag{4}$$

when considering a perforated plate upstream a porous media. $\tilde{\alpha}$ is the dynamic tortuosity of the porous media filling the cavity. ε is calculated from the modal approach for circular apertures on a rectangular pattern and approximated for $\sqrt{\phi} < 0.4$ by [5]:

$$\varepsilon \approx 0.48\sqrt{\pi R_{\text{perf}}^2}(1 - 1.14\sqrt{\phi}), \tag{5}$$

with $R_{\text{perf}} = D_{\text{perf}}/2$, the perforation radius.

This approach has been successfully compared to other models and experimental measurements [7] and is consequently chosen.

Plates with square apertures on square pattern are still modeled following the JCA model by replacing the perforation radius by the hydraulic radius. The hydraulic radius is defined as twice the ratio of the total perforation volume to its surface area. The added length correction is estimated by a modal approach and approximate by [2,5]:

$$\varepsilon \approx 0.48\sqrt{A_{\text{perf}}}(1 - 1.25\sqrt{\phi}), \tag{6}$$

where A_{perf} is the elementary surface of the square aperture. The difference of the constant between Eqs. (5) and (6) is due to the difference between the radiation impedance of a circular aperture on a rectangular pattern and a rectangular aperture on a rectangular pattern [2,5].

For rectangular apertures, the added length correction should be rigorously calculated from Table 1 and Fig. 4 of Ref. [2]. However, assuming a low porosity and a moderate aperture shape factor (width/length), Eq. (6) combined with the hydraulic radius can be used.

3. Numerical simulations

3.1. Influence of perforation diameter

The perforation diameter is known as the main parameter controlling the viscous dissipation of the energy carried out by acoustical waves since it controls the airflow resistivity. Fig. 3 shows the influence of the diameter for a 1 mm-thick single uniform tube (ϕ = 1) of circular cross section backed by a 20 mm-thick plenum. As shown for a single uniform tube backed by a rigid termination [11], the overall sound absorption coefficient increases as the diameter increases until it reaches a climax for a specific diameter D_{spe}, and then decreases. If the diameter is too small, the resistivity is too high, the fluid hardly penetrates the tube and acoustic waves are thus reflected. Conversely, if the diameter is too high, the resistivity is too low and the fluid easily penetrates the tube. Sound absorption is still poor due to the weak viscous dissipations. D_{spe} is the diameter for which the sound absorption coefficient reaches 100% at the first absorption peak. The frequency of this peak depends on the perforation rate as explained in Section 3.2. A specific diameter can be found for each sample thickness L and plenum thickness L_c.

Table 1
Acoustical parameters of downstream porous media.

Porous media	Porosity, ϕ	Airflow resistivity, σ (N sm^{-4})	Viscous carac. length, Λ (μm)	Thermal carac. length, Λ' (μm)	Tortuosity, α_∞	Thermal permeability, k_0' (m^2)	Young modulus, (Pa)	Structural damping	Poisson factor	Volumic mass, (kg m^{-3})
Glass wool 1	0.975	13,000	65	123	1.01					
Glass wool 2	0.97	57,000	27	106	1.02	12×10^{-10}	1.14×10^6	0.1	0	77
Polymeric foam	0.98	2600	348	545	1.06					

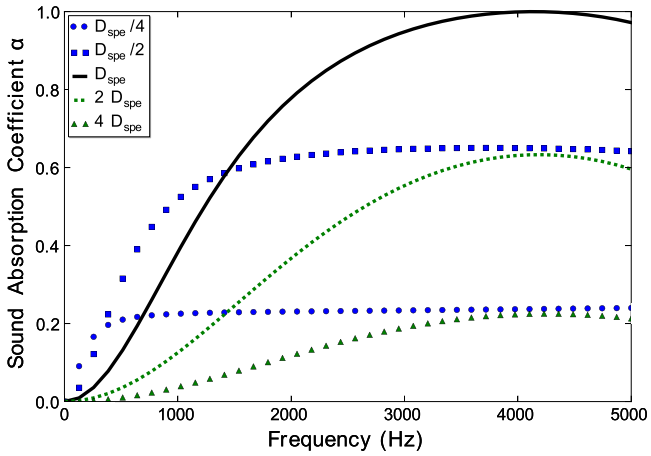

Fig. 3. Effect of diameter of a single cylinder ($\phi = 1$) of circular cross section on sound absorption coefficient for 1 mm-thick cylinder combined with a 20 mm-air plenum.

3.2. Influence of perforation rate

We are now considering a perforated plate backed by an air cavity. Assuming that the dissipation through the perforated plate is mainly controlled by its airflow resistance, the normal surface impedance Z_s of the perforated plate backed by an air cavity can be approximated by:

$$Z_s \approx \sigma L + Z_b. \tag{7}$$

where $Z_b = -j\rho_0 c_0/\tan(k_0 L_c)$ is the surface impedance of the air cavity of thickness L_c. ρ_0, c_0 and k_0 are the density, the speed of sound and the acoustical wavenumber of air, respectively.

The sound absorption coefficient α can be deduced from the normal surface impedance,

$$\alpha = 1 - \frac{|Z_s - Z_0|^2}{|Z_s + Z_0|^2}. \tag{8}$$

Using Eqs. (7) and (8), the sound absorption can be maximized when the specific airflow resistance $(\sigma L)_{spe}$ is equal to the characteristic impedance of the air Z_0:

$$(\sigma L)_{spe} = Z_0. \tag{9}$$

Using Eqs. (2) and (9), the corresponding specific diameter writes:

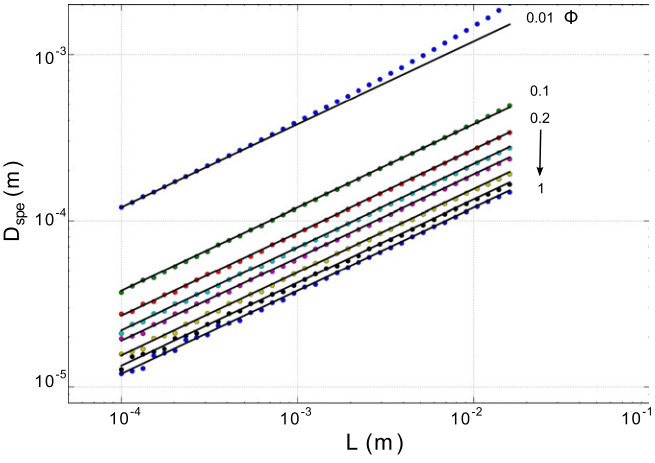

Fig. 4. Relation between specific perforation diameter D_{spe} and thickness of perforated plate L (valid for $L \in [0.1–20]$ mm and $L_c \in [2–200]$ mm). Comparison of Eq. (10) to the simulated values.

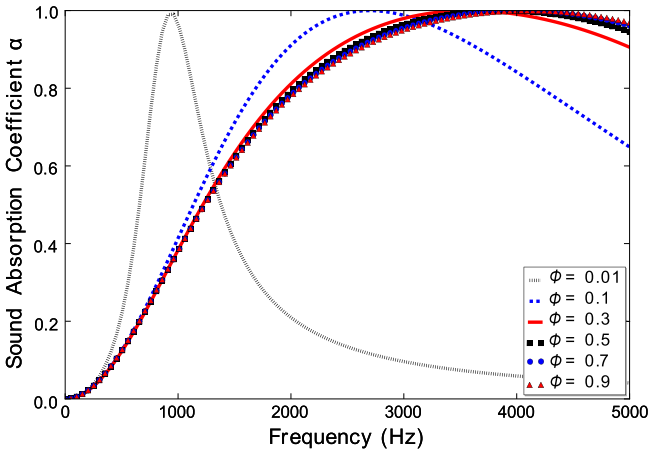

Fig. 5. Effect of perforated rate ϕ ($L = 1$ mm and $L_c = 20$ mm).

$$D_{spe} = \sqrt{\frac{32\eta}{Z_0}}\sqrt{\frac{L}{\phi}} = \beta\sqrt{\frac{L}{\phi}}, \tag{10}$$

with $\beta = 0.0012$ ($m^{1/2}$) for $Z_0 = 409$ (Ns/m^3).

Dry air conditions have been used (20 C, 101.3 kPa) but the typical atmospheric conditions do not significantly change the constant β. Note that β differs from the case of rigid termination [11].

Simulations have shown that Eq. (10) is valid in the ranges [0.1–20] mm and [2–200] mm for L and L_c, respectively. This formula is compared, for different perforation rates, to the simulated values of the specific diameter in Fig. 4 with L in the range [0.1–20] mm and $L_c = 50$ mm. Note that an error can appear for very low perforation rates.

A specific diameter can thus be found for each set of parameters (L, L_c, ϕ). However, the frequency of the peak f_p reaching a maximum sound absorption depends on the perforation rate and the plenum length. Sound absorption coefficients are plotted in Fig. 5 for perforation rates between 0.01 and 0.9. One can note two behaviours of the multilayer (resistive layer – air cavity). For perforation rate over 0.2, the frequency of the peak is approximately given by the quarter wave length which is constrained by the thickness of the plenum:

$$f_p \approx \frac{c}{4L_c}, \tag{11}$$

where c is the speed of the sound in the media filling the plenum. For very low perforation rate, $\phi < 0.1$, the system acts as a Helmholtz resonator. The frequency of the peak is thus controlled by:

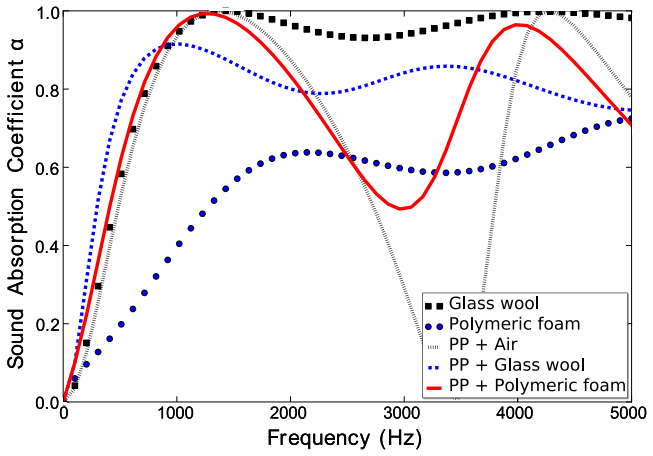

Fig. 6. Effect of media filling cavity ($\phi = 0.1$, $D_{spe} = 120$ μm $L = 1$ mm and $L_c = 50$ mm).

$$f_p \approx \frac{c}{2\pi}\sqrt{\frac{\phi}{(L+2\varepsilon)L_c}}. \quad (12)$$

Eq. (12) is linked to the classical formula of Helmholtz resonator by using $\phi/L_c = A_{perf}/V_c$, with V_c the volume of the cavity.

Note that in both cases, increasing the thickness of the plenum enhances the low frequency sound absorption, however, the selectivity is increased when plenum is filled with air.

3.3. Influence of downstream layer

Previous results have shown that it is possible to optimize a perforated plate or a resistive screen upstream an air cavity. Assuming two parameters among the three (D_{perf}, ϕ, L) are known, the third can be adjusted to maximize the sound absorption. Besides, knowing ϕ and L_c, the frequency of the maximum absorption peak can be predicted. The case of a porous media filling the downstream cavity is now considered. Fig. 6 compares two 50 mm-thick porous materials with and without an optimized perforated plate. A glass wool, known as good sound absorber, and a polymeric foam, with moderate acoustic performances, are used. Their parameters are given in Table 1 (glass wool 1 and polymeric foam). One can note that the addition of a perforated plate, conveniently designed according to Eq. (10) upstream the porous material can enhance mid frequency sound absorption. This phenomenon is due to the bi-permeability of the multilayer screen + glass wool. It has been already observed [6,12] and explained by Rebillard et al. [6]. They explain that the main effect of the resistive screen is to increase the real part of the impedance of the porous material that is close to the airflow resistance σL of the resistive screen. Until the first absorption peak, performances are similar regardless the media filling the cavity (air, glass wool 1, polymeric foam). In fact, under the frequency of the peak f_p, the sound absorption is controlled by the perforated plate (or resistive screen). This result is valid while $(\sigma L)_{downstream} < (\sigma L)_{upstream}$, where σL is the airflow resistance. For higher $(\sigma L)_{downstream}$, the multilayer is too resistive and the sound absorption is thus deteriorated. However, for frequencies upper than f_p, the media filling the cavity plays a role and reduces the sound absorption selectivity. A thick downstream layer is not necessarily advantageous depending of the desired frequency range.

4. Experimental validation

An experimental validation is now carried out on two multilayers with an upstream woven textile screen. It is first combined with a 20 mm-thick air cavity and then with a 20 mm-thick glass wool (glass wool 2 from Table 1). The screen shows rectangular apertures as depicted in Fig. 7a and has a 500-μm-thickness. The perforation rate and the size of apertures are calculated from microscopic analysis by a basic image processing. The result of the image processing is illustrated in Fig. 7b. The perforation rate is obtained by dividing the open surface (black) by the total surface. Length (a) and width (b) of rectangular apertures are measured from the profiles along x and y axis for each aperture and then averaged. An example of aperture profiles are shown in Fig. 8. The average on 12 apertures gives $a = 367 \pm 18$ μm and $b = 74 \pm 12$ μm. The hydraulic radius is thus $\Lambda' = 2\frac{ab}{2(a+b)} = 62 \pm 8$ μm. The screen is still modeled with JCA model. Its thickness is considered equal to fiber thickness (250 μm) because the textile is woven and the perforation length is equal to the fiber thickness instead of the screen one. This microscopic characterization has been successfully compared to two acoustical characterizations from impedance tube measurements [13]. In this method, the static airflow resistivity and the fraction of open area are obtained from analytical expressions and a single measurement of the normal acoustic surface impedance of the screen backed by an air cavity in a standing wave tube. Results are compared in Table 2. The two acoustical characterizations have been carried out for the actual thickness of the screen (500 μm) and for the thickness used in microscopic characterization (250 μm). There is a good agreement for hydraulic radius and airflow resistance (σL) of the screen. Perforation rate and airflow resistivity depend on the chosen thickness but both of them could be used in a JCA model with the associated thicknesses. The characterization method used for the glass wool 2 relies on the direct measurements of the open porosity ϕ [14], the static airflow resistivity σ [15], and the indirect determination of the viscous Λ and thermal Λ' characteristic lengths, the high frequency viscous tortuosity α_∞ and the static thermal permeability k_0' from impedance tube measurements using [16] and [17]. Johnson–Champoux–Allard–Lafarge (JCAL) [8,9,18] fluid equivalent model is used. Note that elastic parameters have to be taken into account in the modeling of glass wool. Acoustic and elastic properties of the glass wool 2 are given in Table 1. Fig. 9 compares experiments and simulations of the multilayer textile + air and the

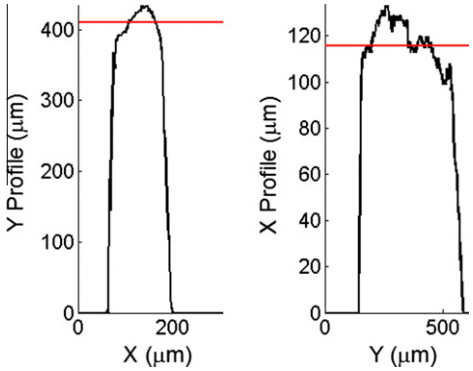

Fig. 8. Example of profiles used for characterizing textile apertures.

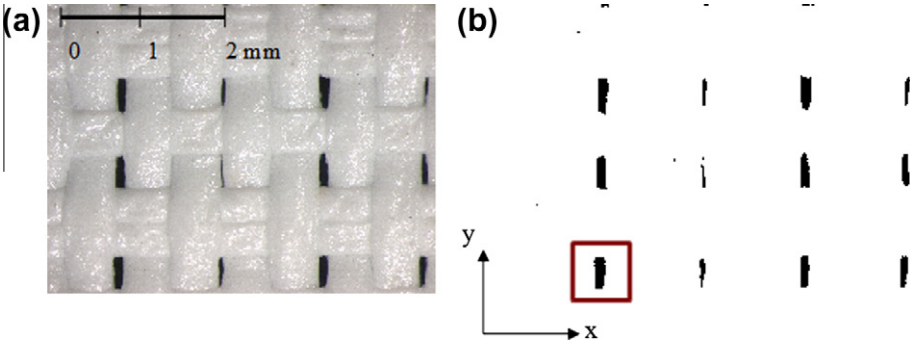

Fig. 7. Woven textile screen (a) and associated image processing (b).

Table 2
Screen characterization.

Parameters	Microscopic characterization	Acoustic characterization 1	Acoustic characterization 2
Thickness L (mm)	0.25	0.5	0.25
Perforation rate ϕ	0.0231	0.0490	0.0281
Airflow resistivity σ (N sm^{-4})	1.66e6	0.79e6	1.49e6
Hydraulic radius Λ' (μm)	62.0	61.4	59.0
Airflow resistance σL (N sm^{-3})	415	395	372.5

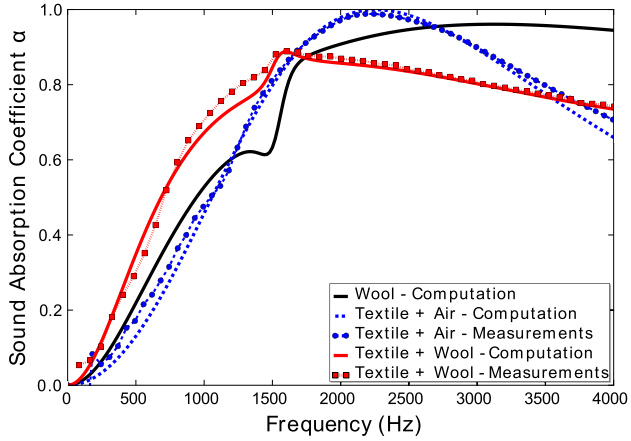

Fig. 9. Sound absorption coefficient of textile layer combined with glass wool and air. Computations versus experiments.

multilayer textile + glass wool 2. The simulation of a single layer of glass wool is also shown. Air cavity and glass wool layer are still 20 mm thick. There is an excellent correlation between measurements and simulations for the multilayers textile–air and textile–glass wool 2. The global sound absorption performance of the multilayer textile + air is similar to the one of textile + glass wool. The low frequency enhancement of the sound absorption of the glass wool combined with the textile screen is captured. Note that the specific diameter for a 250 μm-thick screen with a perforation rate of 0.0231 is $D_{spe} = 125$ μm (or $\Lambda' = 62.5$ μm). The measured hydraulic radius is very close to the specific one. Indeed, Fig. 9 shows that the configuration textile + air is close to the specific configuration as defined in Section 3.

5. Conclusion

A study of multilayer with an upstream resistive layer (perforated plate, resistive screen, etc.) has been proposed. This work highlights a specific perforation diameter for given perforation rate and thickness, which maximizes the normal incidence sound absorption at the first peak. A formula has been established for a wide range of resistive layer parameters. This formula should be a useful guideline for designing resistive layers.

An experimental validation has been successfully carried out on two multilayers textile + air and textile + glass wool. The airflow resistance, the perforation rate and the hydraulic radius of the screen characterized by the microscopic characterization are in good agreement with those of the acoustical characterization.

The main achievement of this work is to set a guideline for designing resistive layer upon a porous media for increasing the sound absorption performance. So, the sound absorption property is easily added to a porous media showing other good properties (thermal, mechanical, etc.). This concept can also be used to value recycled materials.

Moreover, the addition of an upstream resistive layer enables to enhance low frequency sound absorption of a good sound absorber as glass wool. However, this resistive layer has also the effect of decreasing high frequency sound absorption. A special attention should be paid when adding this resistive layer to protect or decorate porous media. Painting or bonding the layer may also have a significant effect by modifying the perforation rate of the screen.

Finally, this study has shown that sound absorption selectivity is increasing when the perforation rate decreases because the considered multilayer tends to act as a Helmholtz resonator. Non-woven textiles, allowing a large perforation rate, should enable wider frequency band sound absorption.

Acknowledgements

Camille Perrot, from Multiscale Modeling and Simulation Laboratory (MSME UMR 8208 CNRS), is gratefully acknowledged for providing micrograph of the textile sample. The author wishes to thank François-Xavier Bécot and Luc Jaouen, from Matelys, for their fruitful discussions and for providing standing wave tube measurements and macroscopic parameters characterization.

References

[1] Ingard KU. Notes on sound absorption technology. Noise control foundation, New York; 1994.
[2] Ingard KU. On the theory and design of acoustic resonators. J Acoust Soc Am 1953;25(6):1037–61.
[3] Beranek LL, Ver IL. Noise and vibration control engineering. New York: Wiley; 1992.
[4] Maa DY. Microperforated wideband absorbers. Noise Control Eng J 1987;29(3):77–84.
[5] Allard JF, Atalla N. Propagation of sound in porous media. Modeling sound absorbing materials. Chichester, UK: Wiley; 2009.
[6] Rebillard P, Allard J-F, Depollier C, Guignouard P, Lauriks W, Verhaegen C, et al. The effect of a porous facing on the impedance and the absorption coefficient of a layer of porous material. J Sound Vib 1992;156:541–55.
[7] Atalla N, Sgard F. Modeling of perforated plates and screens using rigid frame porous models. J Sound Vib 2007;303:195–208.
[8] Johnson DL, Koplik J, Dashen R. Theory of dynamic permeability and tortuosity in fluid-saturated porous media. J Fluid Mech 2007;176:379–402.
[9] Champoux Y, Allard F. Dynamic tortuosity and bulk modulus in air-saturated porous media. J Appl Phys 1991;70(4).
[10] Brouard B, Lafarge D, Allard J-F. A general method of modelling sound propagation in layered media. J Sound Vib 1995;183(1):129–42.
[11] Chevillotte F, Perrot C, Panneton R. Microstructure based model for sound absorption predictions of perforated closed-cell metallic foams. J Acoust Soc Am 2010;128(4).
[12] Duval A, Rondeau J.-F, Deshayes G, Lhuillier F, Bischoff L, Teyssandier B. Generalizes light-weight concept: a comprehensive acoustic package weight reduction strategy. Automotive comfort conference, Le Mans, France; November 15–16, 2006.
[13] Jaouen L, Bécot F-X. Acoustical characterization of perforated facings. J Acoust Soc Am 2011;129(3):1400–6.
[14] Beranek LL. Acoustic impedance of porous materials. J Acoust Soc Am 1942;13:248–60.
[15] A. C-522: Standard test method for airflow resistance of acoustical materials. American Society for Testing and Materials; 2003.
[16] Panneton R, Olny X. Acoustical determination of the parameters governing viscous dissipation in porous media. J Acoust Soc Am 2006;119:2027–40.
[17] Olny X, Panneton R. Acoustical determination of the parameters governing thermal dissipation in porous media. J Acoust Soc Am 2008;123:814–24.
[18] Lafarge D, Lemarinier P, Allard J-F, Tarnow V. Dynamic compressibility of air in porous structures at audible frequencies. J Acoust Soc Am 1997;102:1995–2006.